Optimal Linear Attitude Estimator for Alignment of Point Clouds

Xue Iuan Wong
Mechanical and Aerospace Engineering
University at Buffalo
xuewong@buffalo.edu

Taewook Lee
Mechanical and Aerospace Engineering
University at Buffalo
twlee2@buffalo.edu

Puneet Singla
Aerospace Engineering
Penn State University
pxs433@engr.psu.edu

Manoranjan Majji
Aerospace Engineering
Texas A&M University
mmajji@exchange.tamu.edu

Abstract

This paper presents an approach to estimate the rigid transformation between two point clouds using a linear least squares solution termed as the optimal linear attitude estimator (OLAE). It is shown that by parameterizing the relative orientation between point clouds of interest using the Classical Rodrigues Parameters (CRP), the OLAE approach transforms the nonlinear attitude estimation problem into a linear problem. These linear equations are solved efficiently with closed form solution without any expensive matrix decomposition or inversion. This paper also shows that the 3 degree of freedom (DOF) special case of OLAE that is of interest for aligning point clouds sensed by road vehicles in self-driving car applications can be effectively solved as a linear function with only 1 unknown variable. This formulation enables the 1D RANSAC that can effectively remove outliers in the measurement.

1. Introduction

Advances in microelectronics coupled with Moore's law enabled rapid progress in the sensor technologies to estimate 3D geometry [16, 35]. Estimation of 3D geometry from image and other sensor data has been a topic of interest in the past three decades [26, 15, 21, 46]. The sensed geometry is used by autonomous systems in a wide variety of applications including robotic path planning, terrain mapping, autonomous landing and simultaneous location and mapping [43, 48, 32, 28, 25, 29, 24, 33, 47]. For self driving cars, manufacturing, robotics, planetary exploration, autonomous satellite operations and a variety of proximity operations applications, sensing 3D geometry provides an important modality for relative navigation.

Modern designs of autonomous vehicle systems are usually equipped with multi-camera systems and LIDAR sensing systems. Both of these sensors are capable of generating a densely sample point cloud about its surrounding environment. A multi-camera system solves the point cloud based on multiview geometry [8, 40, 21] and LIDAR directly measures the point cloud with time of flight of a laser beam. The measured point clouds are subjected to various algorithms for application such as object detection[31], 3D mapping[42], odometry[52] etc. Majority of these tasks involve the point cloud registration[37, 34, 3] as an intermediate step. The goal of the point cloud registration is to estimate the transformation between the point clouds such that they can be transformed into a common coordinate system.

The point cloud registration generally comprise two steps. Firstly the point cloud correspondence is determined, and then motion estimation is carried out to compute the transformation. Recent developments on point cloud registration mainly focus on the correspondence problem due to the fact that it has greater impact to the performance of registration.

Iterative closest point(ICP)[4] method assumes the nearest neighbors yield close correspondences. The measurement point clouds with motion estimates are transformed and iteratively updated to improve upon the correspondence estimates. The normal distribution transform (NDT)[5] first partitions the point cloud into a fixed size grid tree. A Gaussian model is then fitted when there are more than 3 points in a grid. Ultimately, the point cloud geometry is transformed into a piecewise linear Gaussian mixture model. This Gaussian mixture model is applied to computes a matching score with the query point cloud, the motion is thus computed as the optimal solution that maximizes the matching score. Another NDT based method known as distribution to distribution matching[45] applies the NDT to both query and template point cloud, the motion is estimated as optimal solution that minimize the L_2 distance between two Gaussian mixture models. LIDAR odometry and mapping(LOAM)[52] extracts edges and planar features from the point cloud and determines the correspondence on a nearest neighbor basis. When the point cloud is generated from multi-cameras system, one can utilize the extra information from image texture for better correspondence estimation. This include the method that utilizes spatial and temporal invariant feature descriptor such as ORB[36, 30], SIFT[27, 2], deep descriptor[7] etc. Methods that utilize the optical flow for feature matching [51, 14, 23], and also direct methods that form the motion estimate and correspondence determination as one optimization problem[12, 11].

Instead of the well studied point cloud correspondence determination problem, this paper focuses on the discussion of the motion estimation part. Given two set of point clouds, the transformation of points is governed by rigid body transformation model.

$$\mathbf{p}_k = R\mathbf{p}_{k-1} + \mathbf{t} \tag{1}$$

where $\mathbf{p}_k \in \mathbb{R}^3$ is the coordinate of a 3D points in k measurement frame specified as Cartesian coordinate, R is a 3×3 rotation matrix, and $\mathbf{t} \in \mathbb{R}^3$ is the translation vector. When the point cloud correspondence is known, motion estimation is computed as the optimal solution that minimizes the least square cost function given in Eq.2.

$$\underset{R,\mathbf{t}}{min} \quad J = \frac{1}{2} || \left[\mathbf{p}_k - R\mathbf{p}_{k-1} - \mathbf{t} \right] ||^2 \tag{2}$$

There is only one optimal solution to the least square cost function, but there are multiple parameterization to the attitude with each of them yielding different properties. Thus, the procedure that solves the optimization problem yields different run-time and numerical precision performance. Common attitude parameterization include but not limited to rotation matrix, Euler angle, quaternion, axis angle, Rodriguez parameters etc.

Euler angles requires 3 parameters to represent the orientation, but it is non-linear and experiences singularities. Due to the non-linearity of Euler angle, Eq.2 is solved with non-linear least square approaches such as Gauss-Newton and Levenberg Marquardt method[10]. Methods that directly apply the rotation matrix consider that each element in matrix R and vector $\mathbf{t}$ as an unknown variable. These methods convert Eq.1 into a set of 12 linear equations and uses the pseudo- inverse to compute the unknown variables[18]. The orthonormal constraint of the rotation matrix is enforced by the nearest orthogonal matrix that uses the singular value decomposition(SVD) of the unknown vector matrix. A different approach introduced by Arun et. al.[1] first compensates the translation thorough the alignment of point cloud centroids and constructs the structure matrix with the point clouds. The product of left and right singular vector matrix of the structure matrix is the rotation matrix. Due to its simplicity and efficiency, Arun's method has been commonly applied to estimates point cloud transformation. The original solution of Arun's method suffered from the mirroring ambiguity. Umeyama[49] solves this issue by ensuring the orientation as proper with determinant of positive 1 of the estimated rotation matrix. A mirror solution that yields a negative determinate value is corrected by flipping the sign of the singular vector that corresponds to the least singular value. A Quaternion parameterizes the attitude with a 4×1 unit vector that is singularity free, but its unit vector constraint is non-linear. Other than the non-linear least square method, Horn [22] introduces a closed form solution to estimate the quaternion from given point cloud measurements, but his method is generally slower than Arun's Method.

This paper proposes a different approach that utilizes Classical Rodriguez parameters (CRP)[41] as an attitude parameterization to solve for the orientation and translation. This method is referred to optimal linear attitude estimator (OLAE). CRP is similar to quaternion, but includes the scalar term with the Euler parameters.

$$\mathbf{q} = [e_1, e_2, e_3]^T tan(\theta/2) \tag{3}$$

where unit vector $[e_1, e_2, e_3]$ is the principle axis of rotation and θ is known as principle angle of rotation. CRP is not favored with respected to quaternion due to its singularity issue when the rotation about the principle axis of rotation at $\pi\ rad$. However, the ICP algorithm requires that the transformation between two point clouds has to be close enough for the nearest neighbor assumption to be valid. This condition implies that the point cloud that satisfy ICP prior condition has to be within the non-singularity range of CRP. CRP and rotation matrix can be converted to each other efficiently with Cayley Transform[9]. Exploiting the unique properties of the CRP along with the unique matrix structure of the pseudo-inverse formulation, we present a method for estimating the transformation between two point clouds that yields a closed form solution while simultaneously giving the exact attitude estimation instead of a nearest orthonormal approximation.

Point cloud measurement is a standard technique for autonomous vehicle system to sense the surrounding environment. Motion model of a road vehicle can be approximated as a planar motion model that has only 3 degree of freedom(DOF) motion, i.e. t_x, t_y, and q_3. One of the most important advantage to utilizes a 3DOF motion model for motion estimation of a road vehicle is the reduction of solution space. Davide[39] introduces a visual odometry algorithm for camera in planar motion with only 1 unknown variable, that leads to a highly efficient 1D RANSAC algorithm for outlier ejection. Inspired by Davide's work, this paper shows that the 3DOF OLAE can be transformed into a linear equation with only 1 unknown variable. This enables the use of iterative robust fitting method such as RANSAC to remove outliers in the measurement.

Our contribution in this paper is the OLAE method that provide accuracy of the iterative methods while maintaining the computational efficiency of a closed form solution, and a 1D function that enables efficient outlier ejection for point cloud measurement from a planar motion platform.

The rest of this paper is organized as follows. Section 2 presents the mathematical detail of the OLAE. Section 3 derive the 3DOF OLAE with 1D outliers ejection. Section 4 shows the experiment result that demonstrate the performance of the proposed algorithm through the ICP registration of point cloud collected from stereo camera and LIDAR sensor. At last we draw the conclusion in section 5.

2. Motion Estimation

Let vector $\mathbf{q} = [q_1, q_2, q_3]$ denote the CRP, the rotation matrix R in term of $\mathbf{q}$ can be obtained with Cayley transform as:

$$R = (I + [\mathbf{q}\times])^{-1} (I - [\mathbf{q}\times]) \tag{4}$$

where $I \in IR_{3\times3}$ is an identity matrix, and operator $[\mathbf{q}\times] \in IR_{3\times3}$ converts a vector into a skew symmetric matrix form written as:

$$[\mathbf{q}\times] = \begin{bmatrix} 0 & -q_3 & q_2 \\ q_3 & 0 & -q_1 \\ -q_2 & q_1 & 0 \end{bmatrix} \tag{5}$$

Substituting Eq.4 into Eq.1, we get:

$$(I + [\mathbf{q}\times])\, \mathbf{p}_k = (I - [\mathbf{q}\times])\, \mathbf{p}_{k-1} + (I + [\mathbf{q}\times])\, \mathbf{t} \tag{6}$$

With some simple manipulation, we can rewrite the Eq.6 into:

$$\mathbf{p}_k - \mathbf{p}_{k-1} = -[\mathbf{q}\times] \left(\mathbf{p}_k + \mathbf{p}_{k-1}\right) + (I + [\mathbf{q}\times])\, \mathbf{t} \tag{7}$$

Note that last term of Eq.7 is a bilinear equation of $\mathbf{q}$ and $\mathbf{t}$, [51] proposed to replace it with a new vector $\mathbf{b} = (I + [\mathbf{q}\times])\, \mathbf{t}$, such that Eq.7 is linear solution and the unknowns $\mathbf{q}$ and $\mathbf{b}$ are solved with pseudo-inverse. Solution of $\mathbf{t}$ is solved in a following step as $\mathbf{t} = (I + [\mathbf{q}\times])^{-1}\, \mathbf{b}$. His method required to invert a 6×6 matrix that leads to efficiency reduction. In order to maintain the efficiency we take the approach of centroid alignment implemented in previous literature[22, 1]. Note that transforming the point clouds to align with their centroid do not completely compensate the translation. However, the least square solution Eq.2 can still converge to the global minimum where the remaining translation effect will be treated as an additive error.

All points at time k and $k-1$ can be centroided using the following relations:

$$\mu = \frac{1}{n} \sum_{i=1}^{n} \mathbf{p}_i \tag{8a}$$

$$\tilde{\mathbf{p}}_i = \mathbf{p}_i - \mu \tag{8b}$$

Two point clouds that are aligned to their centroid is assumed as translation free, i.e. $\mathbf{t} = 0$. Thus, Eq.6 becomes:

$$\tilde{\mathbf{p}}_k - \tilde{\mathbf{p}}_{k-1} \approx -[\mathbf{q}\times] \left(\tilde{\mathbf{p}}_k + \tilde{\mathbf{p}}_{k-1}\right) \tag{9}$$

For sake of compactness, define:

$$\zeta = \tilde{\mathbf{p}}_k - \tilde{\mathbf{p}}_{k-1} \tag{10a}$$

$$\rho = \tilde{\mathbf{p}}_k + \tilde{\mathbf{p}}_{k-1} \tag{10b}$$

By noting that the matrix vector multiplication of a skew symmetric operator can be interchange as $[\mathbf{q}\times]\rho = -[\rho\times]\mathbf{q}$, Eq.6 becomes:

$$\zeta = [\rho\times]\mathbf{q} \tag{11}$$

Note that matrix $[\rho\times]$ is a rank deficient matrix that cannot directly be inverted to calculates $\mathbf{q}$. It requires at least 3 points ($n > 3$) to calculate the least squares solution with the pseudo-inverse. Eq.12 governs the procedure to calculate the pseudo-inverse solution to the point cloud motion estimation.

$$B = \sum_{i=1}^{n} [\rho_i\times]^T [\rho_i\times] \tag{12a}$$

$$C = \sum_{i=1}^{n} [\rho_i\times]^T \zeta \tag{12b}$$

$$\mathbf{q} = B^{-1} C \tag{12c}$$

where B is a 3×3 symmetric matrix that has a closed form solution to its inverse matrix. Combine Eqs.8 and 12, we present the OLAE method that estimates the relative orientation between two point clouds in a computationally efficient manner. Given the estimated CRP, rotation matrix is computed with Cayley Transform with Eq.4 and translation is computed as:

$$\mathbf{t} = \mu_k - R\mu_{k-1} \tag{13}$$

For the remaining of this section, we analyze the runtime performance of the proposed algorithm. The point cloud centroid alignment take $3n$ summation, $3n$ subtraction, and 3 deviation. Calculation of ρ and ζ totally spend

$6n$ summation and subtraction. Matrix B take $6n$ multiplication and $6n+3$ summation after exploiting the sparsity and symmetric properties of the skew symmetric matrix. While calculation of matrix C take additional $6n$ multiplication and $6n$ summation. The 3×3 matrix inversion of a symmetric matrix has complexity of $\Theta(24)$, and the complexity of matrix-vector multiplication is 9. Thus the total complexity of OLAE is $\Theta(42n+42)$

Due to the n matrix-matrix and matrix-vector multiplication in construction of B and C matrix, the presented algorithm do not have significant run-time advantage over to the Arun method that involve only n vector vector outer product and a highly optimized 3×3 SVD decomposition. However, the presented algorithm estimates the precise attitude parameterization in CRP form instead of a nearest orthonormal matrix. This enable a more accurate attitude estimation over the existing closed form solution but more computationally efficient over the iterative based method. This extra accuracy has show improvement in ICP convergence properties that is demonstrated in experiment section.

3. 3DOF OLAE

Assume that the transformation between two sequential point cloud measurement is planar motion. Thus, $\mathbf{t} = [t_x, t_y, 0]$ and $\mathbf{q} = [0, 0, \mathbf{q}_3]$. Let the centroid alignment part remain identical to 6DOF case, we can show that Eq.11 can be rewritten as:

$$\begin{bmatrix} \zeta_1 \\ \zeta_2 \end{bmatrix} = \begin{bmatrix} -\rho_2 \\ \rho_1 \end{bmatrix} q_3 \tag{14}$$

Eq.14 show that after compensates the translation with centroid alignment, the system of equations of 3DOF OLAE reduced to 2 linear equations with only q_3 as unknown. Two equations in Eq.14 can be effectively combine into one straight line equation:

$$\mathbf{y}(\zeta) = q\mathbf{x}(\rho) \tag{15}$$

where $\mathbf{y}(\zeta)$ and $\mathbf{x}(\rho)$ is two $2n\times 1$ vectors with ζ_1, ζ_2, ρ_1, and ρ_2 as variables following to the definition in Eq.14. Thus, estimation of CRP becomes a straight line fitting problem. Eq.15 can be applied to robust fitting algorithm such as RANSAC[13], Least Median of Square[44] to remove outliers, or directly computes the median of all q_3 from Eq.15 as the attitude estimation result.

Planar motion model is only an approximation to the actual vehicle motion model that is not always truth in practice. However, as being pointed out by Davide[39], the planar motion model is still an good approximation model to remove outliers from measurement. A practical approach is to use the RANSAC result of Eq.15 to remove outliers, and utilizes the inliers to Eq.12 to estimate the vehicle motion. The performance of this approach will be demonstrated in experiment section with LIDAR measurement from KITTI dataset.

number of points	OLAE (sec)	Arun (sec)
1e3	0.007	0.007
5e3	0.0017	0.0017
1e4	0.0035	0.0023
1e5	0.0261	0.00218

Table 1: Simulation run time comparison between OLAE and Arun method in sec

4. Experiment

This section show the experiment result of an ICP algorithm that is modified to use OLAE for motion estimation, we only compare our result to the SVD based Arun's method with Umeyama's mirror ambiguity fixed due to the fact that it is the commonly used method in practical ICP application. Firstly, we show a run time comparison between OLAE and Arun method with simulation with known points cloud correspondence. Both methods are tested with a set of randomly generated 3D points and random motion within the ICP range.

The simulation result in Tab.1 shows that OLAE yield no speed advantage to the Arun's method. This was expected result when it come to the simply point to point transformation with no iterative correspondence update. This simulation is performed in Matlab where the algorithm run-time is measured by Matlab's profiling tool.

Next, we present the experimental result for demonstrate the application of OLAE to point clouds registration with measurement from a stereo-camera. Measurement for this experiment is 200 sequential stereo camera frames of a man made simulated terrain inside a laboratory, 3 out of 200 pair of stereo images are shown in Fig.1. The ground truth of this experiment is measured from a VICON motion capture device[50]. The measurement sensor is a calibrated Point Grey Bumblebee XB3 stereo camera[19]. The Stereo Point cloud is estimated with the PCL[38] stereo reconstruction function. The ICP algorithm is a standard ICP with KD-Tree from nanoflann library[6], where the linear algebra function including the SVD for the SVD based method are from Eigen library[20]. Note that the OLAE ICP can serve as an independent simultaneous localization and mapping (SLAM) solution, but the only intention of this implementation is to compare the with the SVD based motion estimation method, and thus is not optimize to compare with the other state of the art SLAM algorithm. During the stereo registration, the relative pose between the stereo frames are first approximated by a visual odometry method. This visual odometry method is a naive implementation that first extract image features with ORB method, performs feature

case	OLAE ICP	Arun ICP
total 200 Frames	300.217 sec	422.2 sec
Avg. ICP iteration per frame ($\sim$ 15e3 Pts.)	16	20

Table 2: Run time comparison between OLAE and Arun method on stereo camera registration experiment

tracking over all four images (Left,Right at time k and k-1) with pyramid LK method. Given the feature track, we estimate the corresponding 3D points location with triangulation, and ultimately use OLAE method to estimate the translation. Due to the inaccurate feature tracking and less number of points involve, the visual odometry output is generally not an accurate measurement of the camera motion. However, it is sufficient to provide an initial guess to transform the point cloud such that the prerequisite of the ICP can satisfied. The initial condition of ICP can also be initialized with identity rotation matrix and zero translation, but ICP with this configuration has potential of convergence failure. The ICP registration with visual odometry as initial condition is solved at every frames, but only every 5 frames the transformed point cloud is save to the global map to save the memory space.

The experiment result is concluded in Tab.2 and Figs.2-3. This experiment results show that ICP with OLAE yield speed advantage over the ICP with SVD based method. Where the reconstructed global 3D surface in Figs.2 show the 3D object reconstructed from ICP algorithm with OLAE and SVD. Fig.3 show the error in estimate camera trajectory from the OLAE and SVD based ICP, the increment in estimation error is due to the odometry drift. The comparison of trajectory error shown in Fig.3 show that the increment of error between each measurement is very similar between two solution, that indicates the accuracy of both algorithm is similar. The large increment of error around 40^{th} frame is a result of sudden increment in motion magnitude. Larger error in 40^{th} frame indicates that the OLAE ICP is able to converge from larger motion offset. Note that measurement from this experiment do not satisfy planar motion

Second set of experiment utilizes the Velodyne LIDAR measurement from KITTI odometry dataset[17]. Unlike the stereo data set, we can not use VO to compute the initial guess for the relative motion. We utilizes the vehicle kinematic assumption to derive the initial guess in this experiment. The vehicle kinematic assumption states that the dynamic properties of the road vehicle under normal operating condition prohibits the dramatic change in its kinematic states. Thus, given a sufficient sampling rate, the vehicle motion at current measurement should be similar to previous measurement. Base on this observation, we can use the previous estimation as the initial guess for current motion estimation. This assumption guarantees the LIDAR measurements satisfy the ICP prerequisite and improve the convergence rate and accuracy of ICP. On the other hand, we remove all LIDAR points with height lower than -1.5m from the raw measurements to removes the ground points that are not useful to the ICP algorithm. An estimated 3D map from LIDAR measurement of KITTI sequence 00 from time step 0-50 second is shown in Figs.4 and the run-time comparison is given in Tab.3. The estimated trajectory comparison of the measurement for 0-200 second is shown in Fig.5. Owing to the fact that the LIDAR do not computes points cloud from expensive stereo matching and a lesser number of points as the result of simple artifact removal based on point height, the run-time of ICP algorithm on LIDAR is much faster then on stereo camera measurement. These experiment results show that OLAE with 1D RANSAC provide the best accuracy over OLAE and SVD but slowest in run time. OLAE yield accuracy improvement while maintaining similar run-time performance over Arun's method. The run-time comparison result in Tab.3 indicates that the increment of runtime of OLAE+1D RANSAC is not only due to the RANSAC algorithm, but also the result of increase ICP iteration. This is due to the fact that 1D RANSAC removes outliers during every ICP iteration, the reduction in number of measurement leads to large variation of residual error. Therefore, the OLAE ICP with 1D RANSAC take longer to achieve convergence criteria.

case	OLAE	Arun	OLAE RANSAC
total run time (sec)	47.897	47.518	107.4957
Avg. ICP iteration per frame	3.386	3.364	5.1540

Table 3: Run time comparison between OLAE+1D RANSAC, OLAE and Arun method on LIDAR measurement of 500 frames

A comparison of the accuracy and run-time performance over 11 KITTI sequences(0-10) with ground truth measurements are summarized in Figs.6-8. Fig.6 show that ICP utilizes OLAE to estimate point cloud transformation yield accuracy improvement, while Figs.7 -8 show that the average and total run-times for ICP with both configurations are similar to each other. Note that the large drift error in sequence 01 was caused by the rotation motion at the first few measurements in the sequence, this initial rotation error leads to relatively large drifting error. In the same figures, we also demonstrate the performance of OALE ICP with 3DOF OLAE outliers ejection. These experiments results show that ICP with 3DOF OLAE outliers ejection greatly improve the overall accuracy. The run-time of ICP with OLAE outliers ejection is higher than the original ICP due to the fact that an extra algorithm is running along with the original implementation.

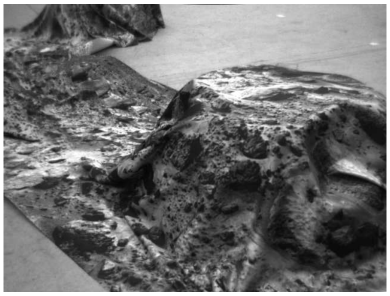

(a) Left frame 1

(b) Left frame 100

(c) Left frame 200

(d) Right frame 1

(e) Right frame 100

(f) Right frame 200

Figure 1: 3 out of 200 pair of stereo images input to experiment

(a)

(b)

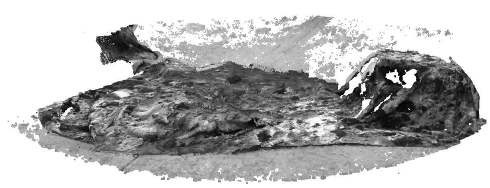

(c)

(d)

Figure 2: 3D object reconstructed by (a-b) SVD ICP, (c-d) OLAE ICP

5. Conclusion and Future work

This paper present the mathematical detail of OLAE and its application ICP registration of point cloud generated from stereo camera. The simulation and experiment result are presented to demonstrate the advantage in run-time and accuracy of the ICP with OLAE over the classical ICP that utilized SVD base motion estimation. We also presents the formulation and experiment result of a 1D RANSAC outliers ejection technique that is based on the 3DOF OLAE.

Current implementation of OLAE ICP does not optimized for real time odometry and localization application but only as a proof of concept to the OLAE ICP. The future work is to expand the application of OLAE to state of the art point cloud registration method that is capable for real time performance.

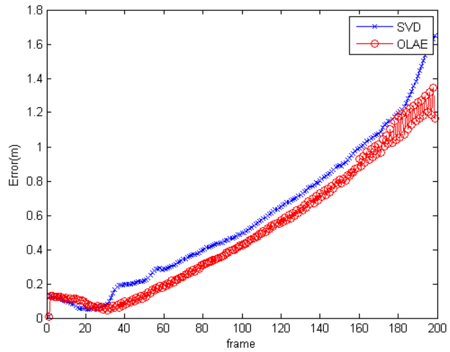

Figure 3: Comparison of trajectory error for stereo point cloud experiment

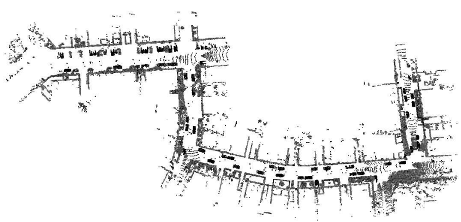

(a)

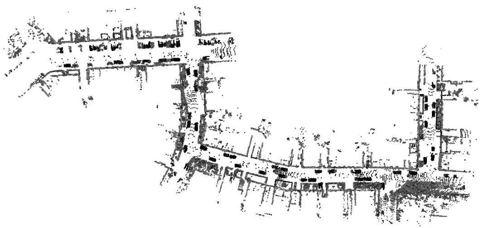

(b)

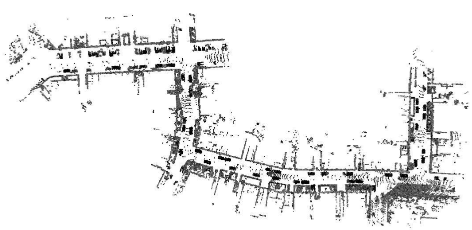

(c)

Figure 4: LIDAR 3D map of KITTI sequence 00 frames 1-500 reconstructed by (a)OLAE ICP + 1D RANSAC (b)OLAE ICP (c) SVD ICP

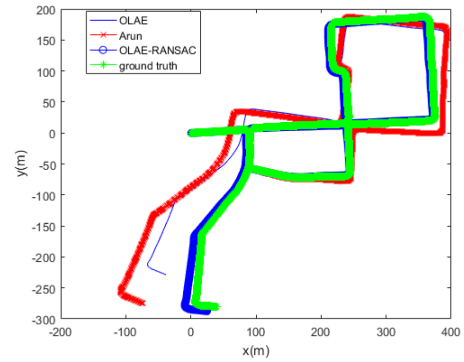

Figure 5: Trajectory comparison of OLAE + 1D RANSAC, OLAE, SVD, and ground truth on LIDAR measurement of KITTI sequence 00 frames 1 - 2000

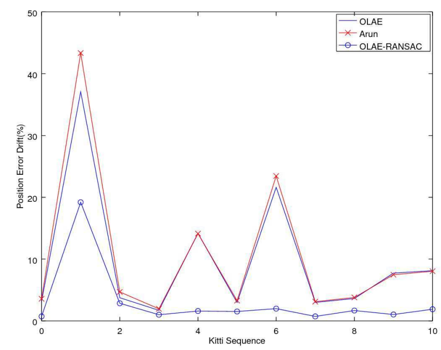

Figure 6: Average position drifting error of OLAE+1D RANSAC, OLAE and SVD ICP on LIDAR measurement of KITTI sequence 0-10

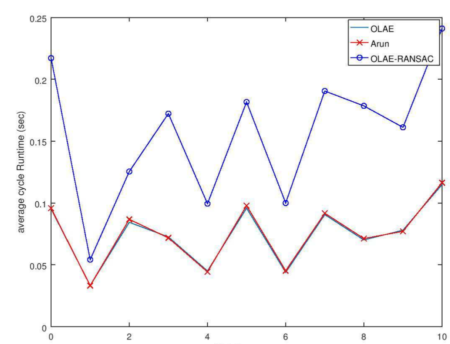

Figure 7: Average run-time comparison(per frame) of OLAE+1D RANSAC, OLAE and SVD ICP on LIDAR Measurement of KITTI sequence 0-10

References

[1] K. S. Arun, T. S. Huang, and S. D. Blostein. Least-squares fitting of two 3-d point sets. *IEEE Transactions on pattern analysis and machine intelligence*, (5):698–700, 1987.

[2] T. D. Barfoot. Online visual motion estimation using fastslam with sift features. In *Intelligent Robots and Systems,*

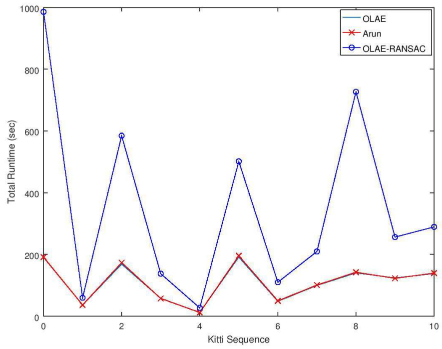

Figure 8: Total run-time comparison of OLAE+1D RANSAC, OLAE and SVD ICP on LIDAR Measurement of KITTI sequence 0-10

2005.(IROS 2005). 2005 IEEE/RSJ International Conference on, pages 579–585. IEEE, 2005.

[3] B. Bellekens, V. Spruyt, R. Berkvens, and M. Weyn. A survey of rigid 3d pointcloud registration algorithms. In *AMBIENT 2014: the Fourth International Conference on Ambient Computing, Applications, Services and Technologies, August 24-28, 2014, Rome, Italy*, pages 8–13, 2014.

[4] P. J. Besl and N. D. McKay. Method for registration of 3-d shapes. In *Sensor Fusion IV: Control Paradigms and Data Structures*, volume 1611, pages 586–607. International Society for Optics and Photonics, 1992.

[5] P. Biber and W. Straßer. The normal distributions transform: A new approach to laser scan matching. In *Intelligent Robots and Systems, 2003.(IROS 2003). Proceedings. 2003 IEEE/RSJ International Conference on*, volume 3, pages 2743–2748. IEEE, 2003.

[6] J. L. Blanco. nanoflann: a c++ header-only fork of flann, a library for nearest neighbor (nn) wih kd-trees, 2014.

[7] S. S. d. C. Botelho, P. L. J. Drews Junior, M. d. S. Figueiredo, C. H. D. Rocha, and G. L. Oliveira. Appearance-based odometry and mapping with feature descriptors for underwater robots. *Journal of the Brazilian Computer Society*, 15(3):47–54, 2009.

[8] M. Z. Brown, D. Burschka, and G. D. Hager. Advances in computational stereo. *IEEE Transactions of Pattern Analysis and Machine Intelligence*, 25(8):993–1008, August 2003.

[9] S. D. CAYLEY et al. *The collected mathematical papers*. 1894.

[10] J. Crassidis and J. Junkins. *Optimal Estimation of Dynamic Systems*. Applied mathematics and nonlinear science series. CRC Press, Boca Raton, FL, 2nd edition, 2011.

[11] J. Engel, V. Koltun, and D. Cremers. Direct sparse odometry. *IEEE transactions on pattern analysis and machine intelligence*, 40(3):611–625, 2018.

[12] J. Engel, J. Stückler, and D. Cremers. Large-scale direct slam with stereo cameras. In *Intelligent Robots and Systems (IROS), 2015 IEEE/RSJ International Conference on*, pages 1935–1942. IEEE, 2015.

[13] M. A. Fischler and R. C. Bolles. Random sample consensus: a paradigm for model fitting with applications to image analysis and automated cartography. In *Readings in computer vision*, pages 726–740. Elsevier, 1987.

[14] C. Forster, M. Pizzoli, and D. Scaramuzza. Svo: Fast semi-direct monocular visual odometry. In *Robotics and Automation (ICRA), 2014 IEEE International Conference on*, pages 15–22. IEEE, 2014.

[15] D. Forsyth and J. Ponce. *Computer Vision: A Modern Approach*. Prentice Hall, Englewood Cliffs, NJ, 2003.

[16] T. Geibig, A. Shoyketbrod, A. Hommes, R. Herschel, and N. Pohl. Compact 3d imaging radar based on fmcw driven frequency scanning antennas. In *Proceedings of the 2016 IEEE Radar Conference*. IEEE Radar Society, 2016.

[17] A. Geiger, P. Lenz, and R. Urtasun. Are we ready for autonomous driving? the kitti vision benchmark suite. In *Conference on Computer Vision and Pattern Recognition (CVPR)*, 2012.

[18] J. C. Gower and G. B. Dijksterhuis. *Procrustes problems*, volume 30. Oxford University Press on Demand, 2004.

[19] P. Grey. Point grey bumblebee® xb3, 2014.

[20] G. Guennebaud, B. Jacob, et al. Eigen: a c++ linear algebra library. *URL http://eigen. tuxfamily. org, Accessed*, 22, 2014.

[21] R. I. Hartley and A. Zisserman. *Multiple View Geometry in Computer Vision*. Cambridge University Press, ISBN: 0521623049, 2000.

[22] B. K. Horn. Closed-form solution of absolute orientation using unit quaternions. *JOSA A*, 4(4):629–642, 1987.

[23] X. Iuan Wong and M. Majji. Uncertainty quantification of lucas kanade feature track and application to visual odometry. In *Proceedings of the IEEE Conference on Computer Vision and Pattern Recognition Workshops*, pages 10–18, 2017.

[24] A. Johnson, Y.Cheng, and L. Matthies. Machine vision for autonomous small body navigation. *Proccedings of the IEEE Aerospace Conference*, pages 661–671, 2000.

[25] J. L. Junkins, M. Majji, B. Macomber, J. Davis, J. Doebbler, and R. Noster. Small body proximity sensing with a novel hd3d ladar system. In *Proceedings of the 33rd Annual AAS Guidance and Control Meeting, Breckenridge, CO; UNITED STATES;*, Advances in Astronautical Sciences, page AAS 11=054. American Astronautical Society, Univelt Publications, January 2011.

[26] D. L. Light. *Manual of Photogrammetry*. American Society of Photogrammetry, Falls Church, Virginia, 4 edition, 1980.

[27] D. Lowe. Distinctive image features from scale invariant keypoints. *International Journal of Computer Vision*, 20(2):91–110, 2004.

[28] M. Majji, J. Davis, J. Doebbler, B. Macomber, J. L. Junkins, M. Vavrina, and J. Vian. Terrain mapping and landing operations using vision based sensors. In *Proceedings of the AIAA Guidance, Navigation and Control Conference and Exhibit*, Portland, OR, August 2011. AIAA.

[29] H. Moravec. Obstacle avoidance and navigation in the real world by seeing a robot rover. Internal report, The Robotics Institute: Carnegie Mellon University, Pittsburg, PA, 1980.

[30] R. Mur-Artal and J. D. Tardós. Orb-slam2: An open-source slam system for monocular, stereo, and rgb-d cameras. *IEEE Transactions on Robotics*, 33(5):1255–1262, 2017.

[31] J. Niemeyer, F. Rottensteiner, and U. Soergel. Contextual classification of lidar data and building object detection in urban areas. *ISPRS journal of photogrammetry and remote sensing*, 87:152–165, 2014.

[32] C. F. Olson, L. H. Matthies, J. R. Wright, R. Li, and K. Di. Visual terrain mapping for mars exploration. *Computer Vision and Image Understanding*, 105:73–85, 2007.

[33] M. Pollyfeys and L. Van-Gool. From images to 3d models.

[34] F. Pomerleau, F. Colas, R. Siegwart, et al. A review of point cloud registration algorithms for mobile robotics. *Foundations and Trends® in Robotics*, 4(1):1–104, 2015.

[35] A. Revere. Texas instruments: Opt8241 3d time-of-flight (tof) sensor. *Axiom*, 4(1), 2016.

[36] E. Rublee, V. Rabaud, K. Konolige, and G. Bradski. Orb: An efficient alternative to sift or surf. In *Computer Vision (ICCV), 2011 IEEE international conference on*, pages 2564–2571. IEEE, 2011.

[37] S. Rusinkiewicz and M. Levoy. Efficient variants of the icp algorithm. In *3-D Digital Imaging and Modeling, 2001. Proceedings. Third International Conference on*, pages 145–152. IEEE, 2001.

[38] R. B. Rusu and S. Cousins. 3d is here: Point cloud library (pcl). In *Robotics and automation (ICRA), 2011 IEEE International Conference on*, pages 1–4. IEEE, 2011.

[39] D. Scaramuzza. 1-point-ransac structure from motion for vehicle-mounted cameras by exploiting non-holonomic constraints. *International journal of computer vision*, 95(1):74–85, 2011.

[40] D. Scharstein and R. Szeliski. A taxonomy and evaluation of dense two frame stereo correspondence algorithms. *International Journal of Computer Vision*, 47(1/2/3):7–42, April - June 2002.

[41] H. Schaub and J. L. Junkins. Stereographic orientation parameters for attitude dynamics: A generalization of the rodrigues parameters. *Journal of the Astronautical Sciences*, 44(1):1–19, 1996.

[42] B. Schwarz. Lidar: Mapping the world in 3d. *Nature Photonics*, 4(7):429, 2010.

[43] S. Se, D. Lowe, and J. Little. Mobile robot localization and mapping with uncertainty using scale-invariant visual landmarks. *International Journal of Robotics Research*, pages 735–758, 2002.

[44] D. Simpson. Introduction to rousseeuw (1984) least median of squares regression. In *Breakthroughs in Statistics*, pages 433–461. Springer, 1997.

[45] T. Stoyanov, M. Magnusson, and A. J. Lilienthal. Point set registration through minimization of the l 2 distance between 3d-ndt models. In *Robotics and Automation (ICRA), 2012 IEEE International Conference on*, pages 5196–5201. IEEE, 2012.

[46] R. Szeliski. *Computer Vision: Algorithms and Applications*. Springer, 2011.

[47] S. Thrun, W. Burgard, and D. Fox. *Probabilistic Robotics*. MIT Press, 2005.

[48] N. Trawny, A. I. Mourikis, S. I. Roumeliotis, A. E. Johnson, and J. F. Montgomery. Vision aided inertial navigation for pin-point landing using observations of mapped landmarks. *Journal of Field Robotics*, 2006.

[49] S. Umeyama. Least-squares estimation of transformation parameters between two point patterns. *IEEE Transactions on pattern analysis and machine intelligence*, 13(4):376–380, 1991.

[50] vicon. Motion capture system : Vicon, 2018.

[51] X. I. Wong and M. Majji. Extended kalman filter for stereo vision-based localization and mapping applications. *Journal of Dynamic Systems, Measurement, and Control*, 140(3):030908, 2018.

[52] J. Zhang and S. Singh. Loam: Lidar odometry and mapping in real-time. In *Robotics: Science and Systems*, volume 2, 2014.